nature cell biology

DOI: 10.1038/ncb2119

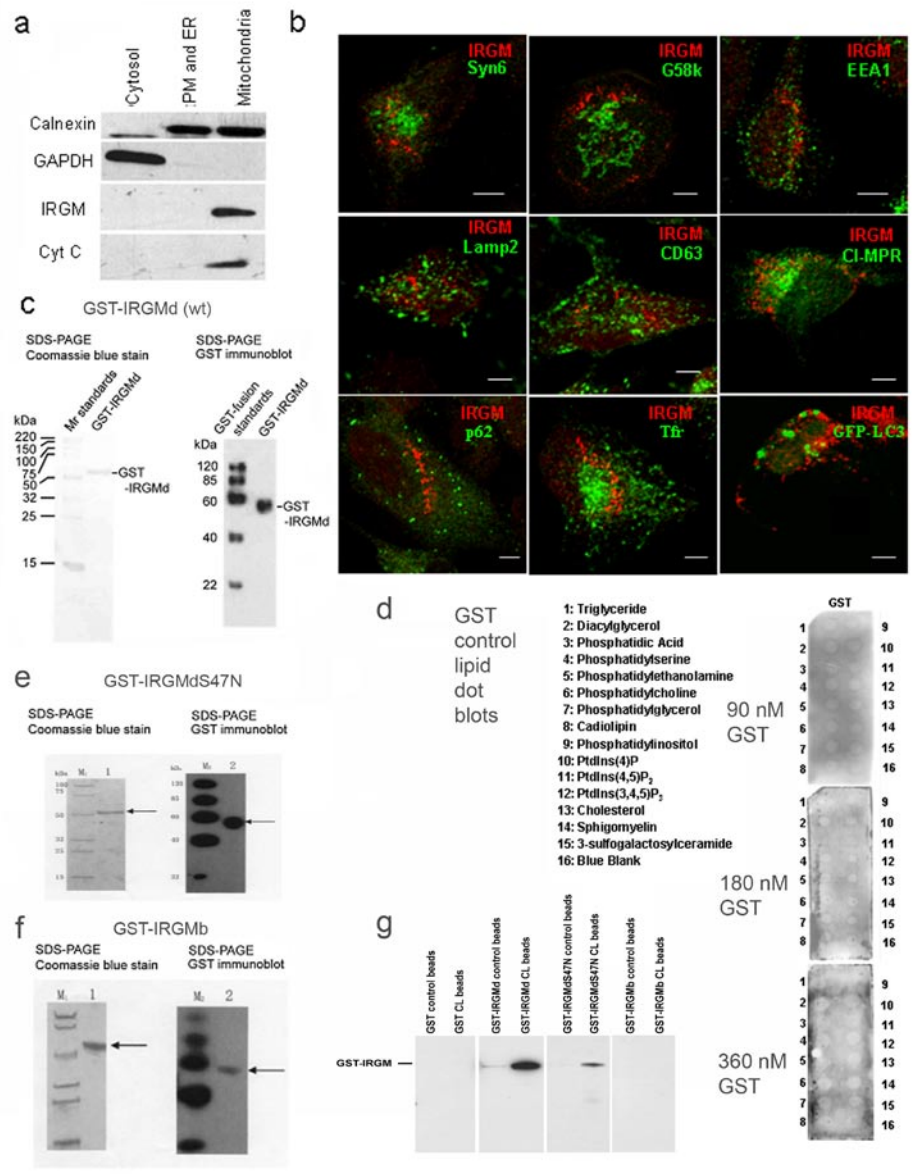

Figure S1 Analysis of IRGM localization, GST-IRGMd, GST-IRGMdS47N and GST-IRGMb protein purification, and analysis of their binding to cardiolipin. a. Mitochondria were purified by Qproteome Mitochondria Isolation Kit (Qiagen) and the fractions were analyzed by immunoblotting with IRGM, calnexin, GAPDH and cytochrome c (CytC) antibodies. b. Immunofluorescence microscopy analysis of endogenous IRGM vis-à-vis indicated intracellular markers. HeLa cells were analyzed by confocal microscopy using primary antibodies to different subcellular markers followed by secondary antibodies conjugated to Alexa 543 for IRGM and Alexa 488 for other markers: Syn6, syntaxin 6 (trans-Golgi network); G58k, Golgi 58 kDa protein (Golgi); EEA1, early endosomal auto-antigen 1 (early endosomes); Lamp2, lysosomal glycoprotein (lysosomes); CD63, late endosomal tetraspanin (late endosomes); CI-MPR, cation-independent mannose-6-phosphate receptor (late endosome); p62, ubiquitinated cargo adapter for delivery of protein aggregates to autophagosoes (autophagic organelles and protein aggregates); Tfr, transferring receptor (recycling endosome); GFP-LC3, autophagosomes. c. GST-IRGMd was overexpressed in E. coli and purified by affinity chromatography. Shown are final protein preparations analyzed by SDS-PAGE and stained with coomassie blue or immunobloted and probed for GST. d. GST control for concentration-dependent analysis of GAT-IRGMd, GST-IRGMdS47N and GST-IRGMb binding to lipids on strip blots (numbers identify lipid dots) shown in Fig. 4g. e,f. GST-IRGMdS47N and GST-IRGMb were overexpressed in E. coli and purified by affinity chromatography. Shown are protein preparations analyzed by SDS-PAGE and stained with coomassie blue or immunoblotted and probed for GST. g. Comparison of GST-IRGMd, GST-IRGMdS47N, and IRGMb binding to cardiolipin agarose beads (see Fig. 4f and Methods).

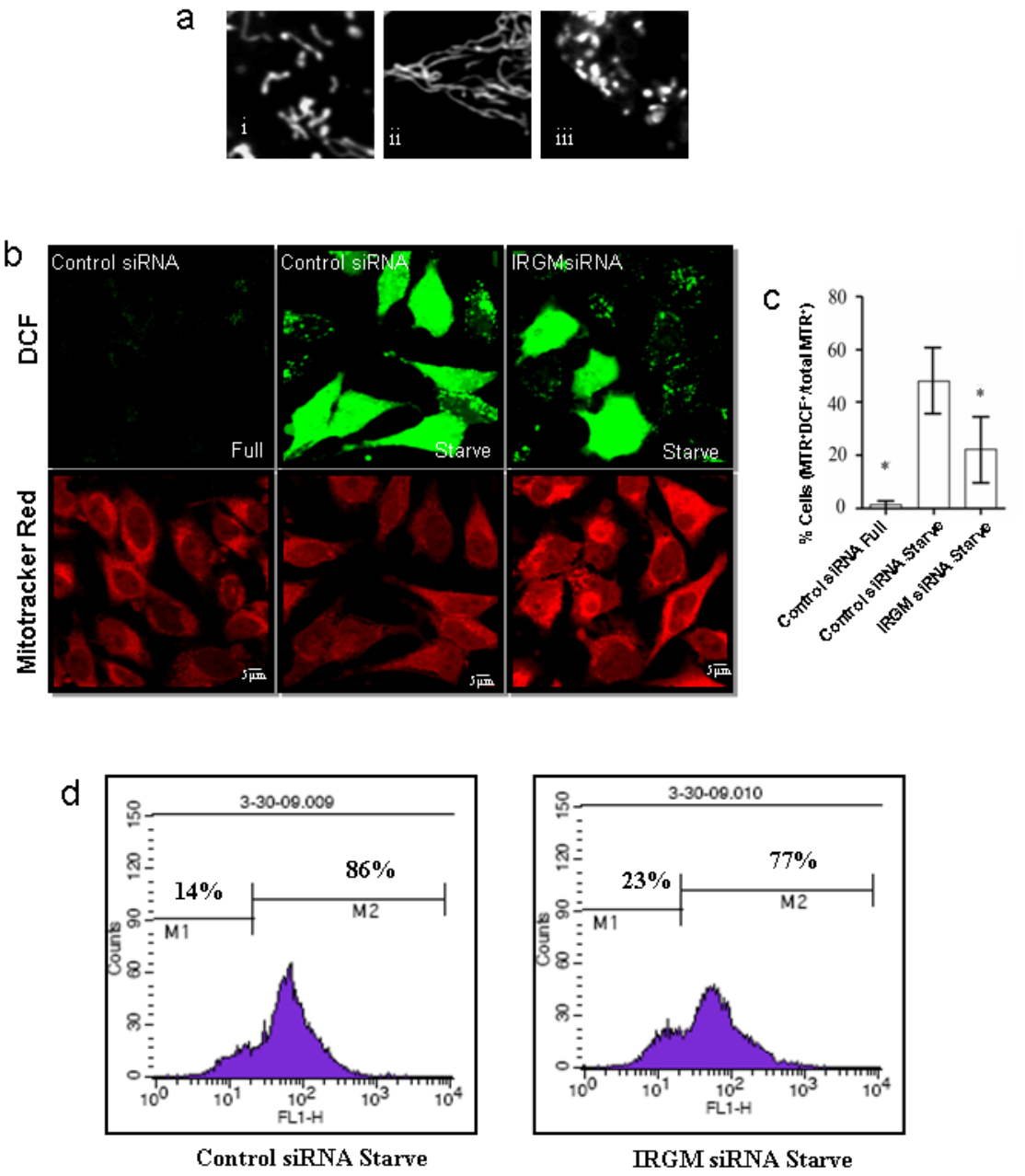

Figure S2 Mitochondrial morphotypes and reactive oxygen species production by mitochondria. a Mitochondrial morphotypes. (i) Normal, (ii) Elongated, (iii) Dots/punctiform. Examples shown are form HeLa cells. Definitions of cellular mitochondrial morphotypes applied throughout this study were as follows: Three distinct mitochondrial morphologies within cells (normal, elongated, dots) were used to count a cell as having normal mitochondria, elongated or punctiform/dots [1-3] based on displaying predominantly one of the three mitochondrial architecture morphotypes (with the threshold of >50%). Data for morphotypes (% of total cells) were obtained in 3 independent experiments, 50 or more cells counted for each experiment. b-d. IRGM affects ROS production in cells subjected to induction of autophagy by starvation. b. HeLa cells were treated with control or IRGM siRNA and subjected to starvation for 3 h. Subsequently, cells were labeled with DCF (30 μm) and MTR (250 nM) for 10 min, washed and fixed with 2% PFA and analyzed by microscopy. c. Quantification of MTR^+DCF^+ positive cells, expressed as % of total MTR^+ cells. Data, means ± SEM (n=3); * $P<0.05$ (t-test). d. Flow cytometry data showing DCF^+ positive cell population (M2) vs DCF^- cell popuation (M1) in cell cultures induced for autophagy by starvation and subjected to siRNA knockdowns as in Fig. 2a. M2 to M1 shift reflects fewer DCF fluorescing cells as a result of lower conversion of the nonfluorescent precursor H_2DCF to its fluorescent oxidation product DCF.

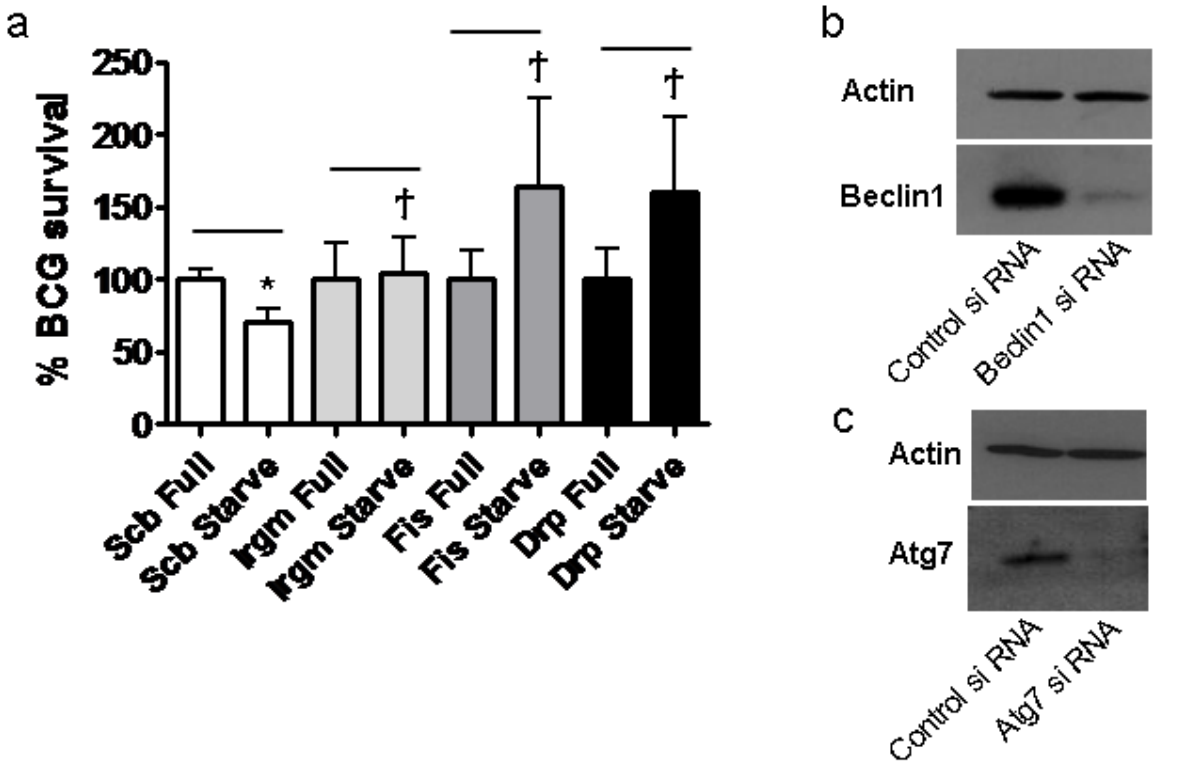

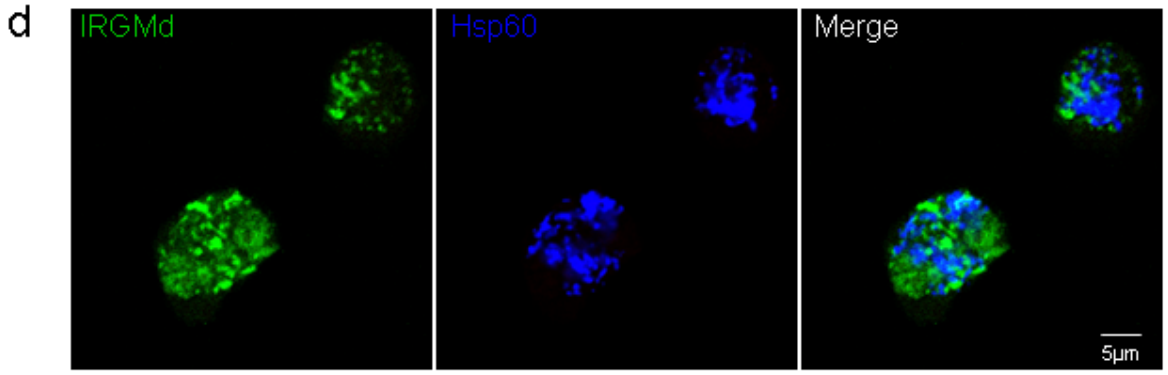

Figure S3 Mitochondrial fission factors affect BCG survival in infected macrophages, knockdowns of autophagy factors and presence of depolarized mitochondria in IRGMd-tarnsfected cells. a. Mitochondrial fission factors and autophagic control of M. tuberculosis var. bovis BCG. U937 cells were transfected with indicated siRNAs and infected with BCG and bacterial viability assay was carried out as described [4]. Data, means ± SEM (n≥3). †P≥0.05,*P<0.05. b and c. Analysis of siRNA knockdowns of autophagy proteins. Cells were transfected with control siRNA or with siRNA to Beclin1 or Atg7 for 48 h. Protein samples were analyzed by Western blotting with anti-Beclin 1 or anti-Atg7 antibodies. Actin, loading control. d. Loss of MTR staining does not represent complete elimination of mitochondria or mitochondrial material. Cells transfected with IRGMd for 48 h still stain for mitochondrial proteins ($Hsp60^{+}$) although they have lost membrane potential (MTR^{-}). Note that cells stained negative for MTR but were positive for Hsp60.

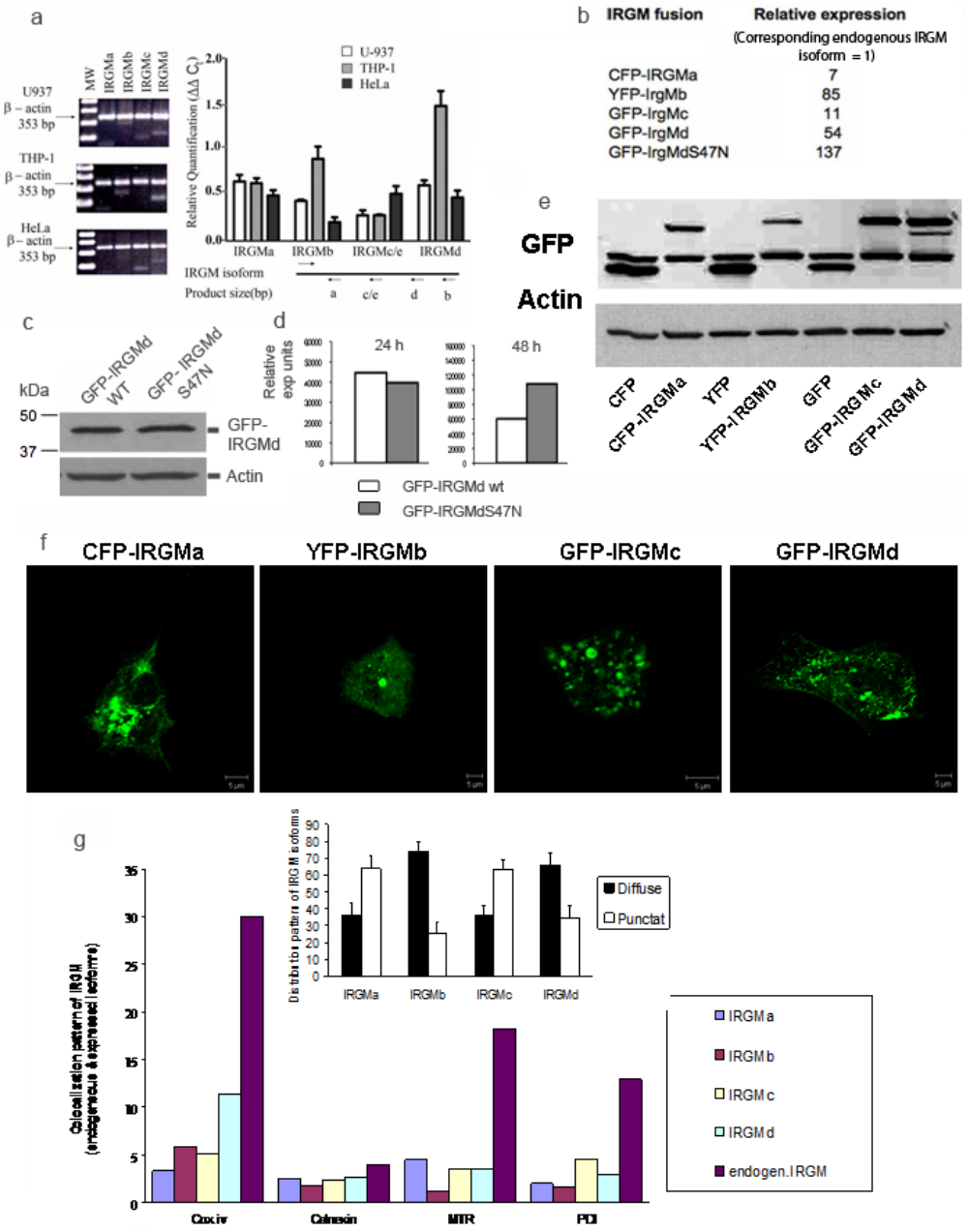

Figure S4 Expression analysis of endogenous IRGM isoforms, expression analysis of fusions between IRGM isoforms and fluorescent proteins, and analsysis of intracellular localization of IRGMd isoforms. a. RT-PCR analysis of endogenous IRGM isoform expression (see Fig. 4a for map) in epithelial HeLa cells, and differentiated U937 and THP1 macrophage-like cell lines. Relative quantification: IRGM mRNA isoform abundance for each specific isoform vs. total IRGM mRNA was calculated as $\Delta\Delta Ct = (C_t^{IRGMi} - C_t^{actin}) - (C_t^{total\ IRGM} - C_t^{actin})$ where i = IRGMa, IRGMb, IRGMc or IRGMd. b-g. Cells (HeLa or 293T) were transfected with fluorescent protein fusions with IRGMa, IRGMb, IRGMc, IRGMd (wild type – wt or no markings, or S47N mutant) for 24 h (or 48 h when indicated). Following transfection with isoform constructs as indicated, cells were either lysed and RNA extracted for RT-PCR analysis (b,d), samples were analyzed by Western blotting using anti-GFP antibodies (c,e) or analyzed by confocal microscopy (f,g). b. Numbers (left column), expression (determined by RT-PCR) of recombinant constructs (fluorescent protein – IRGM isoform fusion) in transfected cells relative to expression of the corresponding endogenous IRGM isoform in untransfected cells (expression of endogenous isoforms is shown in panel a). In transfected cells, expression of endogenous isoforms showed variations ranging from 2-66% of total IRGM, with the exception of IRGMd which ranged within 20-40%. c. Western blot analysis of relative expression and stability at the protein level of GFP-IRGMd wt and GFP-IRGMdS47 mutant. d. Quantitative analysis by RT-PCR of expression at the RNA level of GFP-IRGMd wt and GFP-IRGMdS47 mutant (as in b, only at two different time points as indicated). e. Analysis of fluorescent protein fusions with all IRGM isoforms. Note: anti-GFP antibodies recognize other fluorescent GFP derivatives (CFP and YFP. f. Expression of fluorescent protein fusions with IRGM isoforms assessed by confocal microscopy. g. Analysis of intracellular distribution and localization of IRGM isoforms. HeLa cells were transfected with different IRGM isoforms fused with fluorescent proteins and after 24 h cells were analyzed for distribution (inset; % cells with predominant distribution) as diffuse cytosolic or punctate and for colocalization (% of profiles) with indicated markers (COX IV, mitochondria; Calnexin, ER membrane protein; MTR, polarized mitochondria; PDI, protein disulfide isomerase, ER lumenal protein). For comparison, endogenous IRGM (revealed with IRGM antibody) was included. Number of cells, >100; number of profiles per cell, >10.

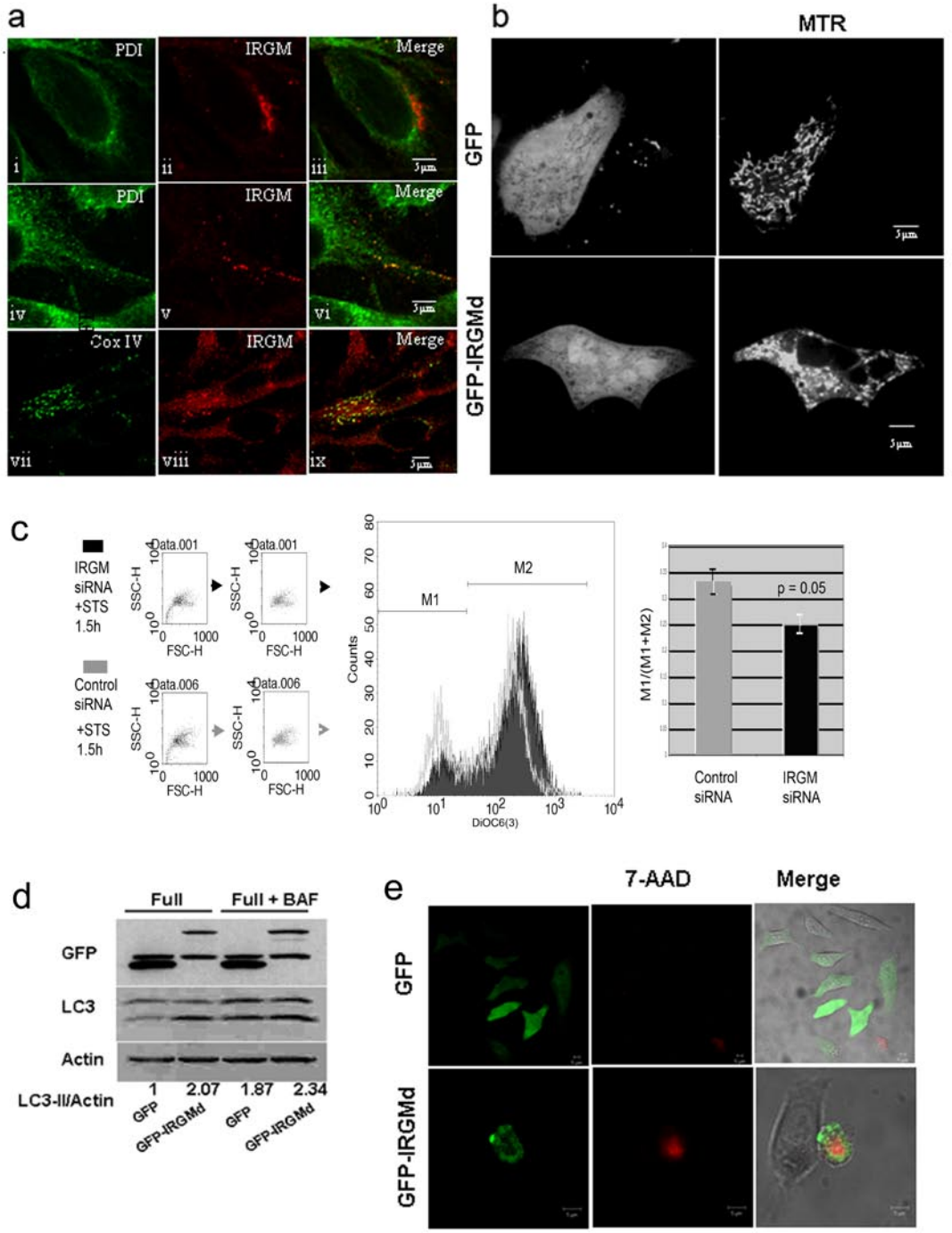

Figure S5 Endogenous IRGM distribution relative to PDI and COX IV effects of IRGM on mitochondrial fragmentation and membrane potential, effects of autophagy, and cell death. a. Confocal microscopy images showing PDI and COX IV distribution relative to endogenous IRGM. Two types of staining patterns of PDI were found relative to IRGM: One with ribbon-like pattern that did not colocalize with IRGM (i-iii) and another one with punctate pattern of PDI that partially colocalized with IRGM (iv-vi; insets, enlarged area demarcated by thin square. Panels vii-ix show endogenous IRGM colocalization with COX IV (mitochondria). b. HeLa cells were transfected with GFP-IRGMd for 24 h, labeled with MTR and imaged by UltraView LCI microscope system (PerkinElmer Life Sciences) showing mitochondrial fragmentation and clumping. c. Knockdown of endogenous IRGM transiently protects mitochondria from staurosporine (1.2 μM) induced depolarization (measured by DiO6(3) fluorescence [5]). Filled box, IRGM siRNA; gray box, control (scrambled) siRNA. Dot plots: total cell population subjected to flow cytometry (left); gated cells analyzed for DiOC6(3) fluorescence (right). M1, depolarized mitochondria, M2, polarized mitochondria. Note a "right shift" of the M2 peak and decrease in the M1 peak in cells treated with IRGM siRNA relative to cells with control (scrambled) siRNA. Effects of IRGM knockdown on mitochondrial depolarization (relative to control siRNA) were observed at 1.5 h (graph) and were lost at 3 h (not shown). d. Cells were transfected with either GFP or GFP-IRGMd for 24 h. Cells were incubated with or without 100 nM Bafilomycin A for 2 h. Cells were lysed and lysates subjected to Western blotting with LC3 antibody to assess autophagy levels. GFP antibody was used to check the level of transfections. e. HeLa cells transfected with GFP or GFP-IRGMd for 48 h were stained with 7-AAD to assess viability (7AAD$^-$, live cells; 7AAD$^+$, dead cells).

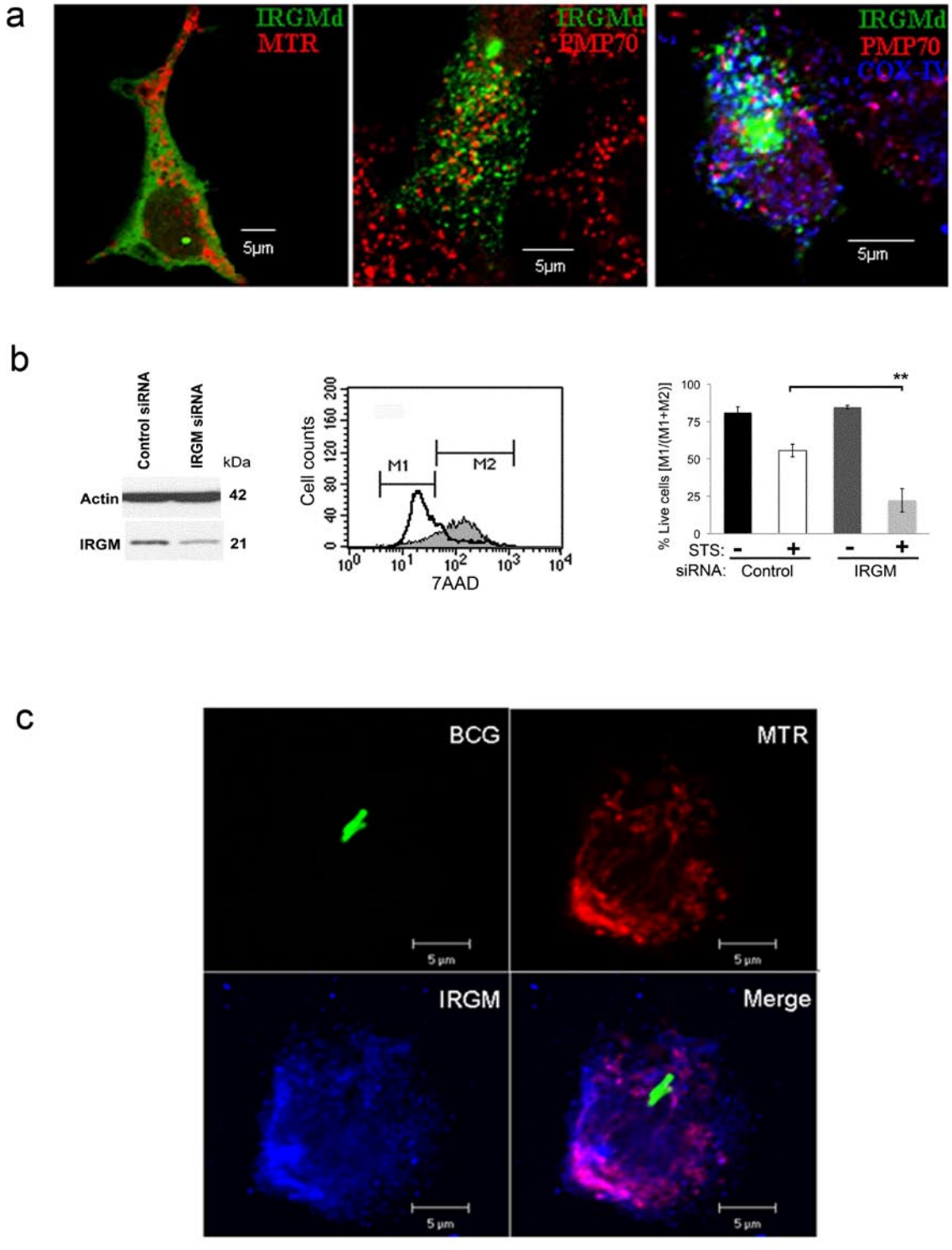

Figure S6 Relationship of IRGMd vis-à-vis mitochondira and peroxisomes, role of endogenous IRGM in cell death, and absence of IRGM form mycobacterial phagosomes. a. IRGMd colocalizes with peroxisomes in addition to mitochondria. HeLa cells were transfected with IRGMd for 24 h and analyzed by immunflourescence using anti-PMP70 (peroxisome marker) alone or anti-PMP70 and anti-COX-IV antibodies, followed by secondary antibodies conjugated to Alexa 543 and 647 respectively. The mitochondrial fission protein Drp1 is known to colocalize with peroxisomes in addition to mitochondria [6, 7]. b. IRGM knockdown (immunoblot) promotes staurosporine (STS; 1.2 μM) induced cell death (measured by 7AAD staining). c. Endogenous IRGM does not directly localize to mycobacterial (BCG; green) phagosomes.

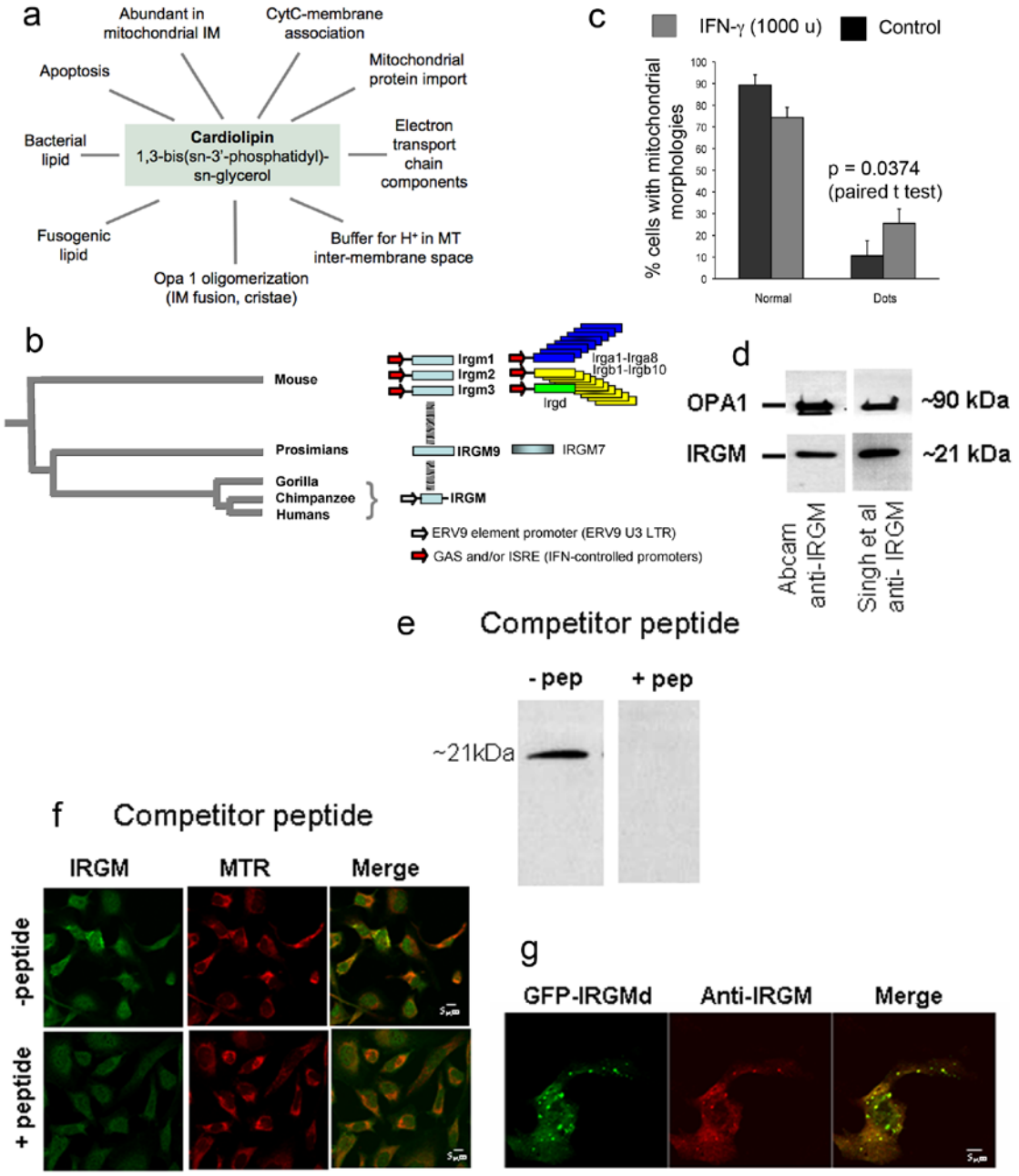

Figure S7 Cardiolipin functions, IRGM phylogeny, effect of IFN-γ on mitochondrial dynamics, and properties of IRGM antibody. a. Cardiolipin properties and functions have been recently reviewed [8]. Cardiolipin localizes predominantly to mitochondrial inner membrane [8]. It is also found in bacteria [8]. Cardiolipin binds to cytochrome c [9] (cytochrome c release from mitochondria is facilitated by cardiolipin oxidation [9] during apoptosis [10]) and many of the membrane proteins involved in electron transport chain and ATP synthesis [8]. It has proton buffering capacity due to an anomalously high pK of one of the phosphate groups [8]. Cardiolipin affects co-assembly into dimers and function of inner membrane fusion protein Mgm1 (yeast equivalent of Opa1) [11], and controls protein import into mitochondria [12]. b. Evolution [13] of IRG (immunity related GTPases): Mouse has 22 IRGs, with 3 related Irgm1, Irgm2, and Irgm3 genes corresponding to IRGM9 in prosimian evolution, a precursor via a number of truncation events and molecular reconstitution of the open reading frame encoding IRGM in antropomorhs. Gorilla, chimpanzee and humans have only one IRG of this category (represented by 24 murine genes). The transcription regulatory elements have also been changed, including replacement of interferon-responsive elements GAS and ISRE (red arrows) in murine genes, with ERV9 retroviral element and transcription form the ERV9 U3 LTR (open arrows). Human polymorphisms associated with susceptibility to tuberculosis and risk for Crohn's disease include the promoter region of IRGM [14, 15]. c. IFN-γ (high dose; 1,000 u) induces detectable mitochondrial fragmentation. IFN-γ at 300 u does not show statistical significance (not shown). d. Comparison of custom made IRGM antibody [16] with the commercial (Abcam) anti-IRGM antibody. Mitochondria were purified using Qproteome mitochondria isolation kit and probed for IRGM. OPA1 was used a positive control for mitochondrial proteins. e. IRGM antibody [16] (2 µg/ml) was incubated in the absence or presence of immunizing peptide (4 µg/ml) at 4°C overnight prior to staining of immunoblot. f. Immunizing IRGM peptide competes for immunoflorescent staining of endogenous IRGM. Note that when competitor peptide was used, cells no longer showed IRGM staining on mitochondria; instead, cells had a diffuse staining for IRGM. g. HeLa cells were transfected with GFP-IRGMd for 24 h, and stained with anti-IRGM antibody followed by Alexa Flour 595 secondary antibody.

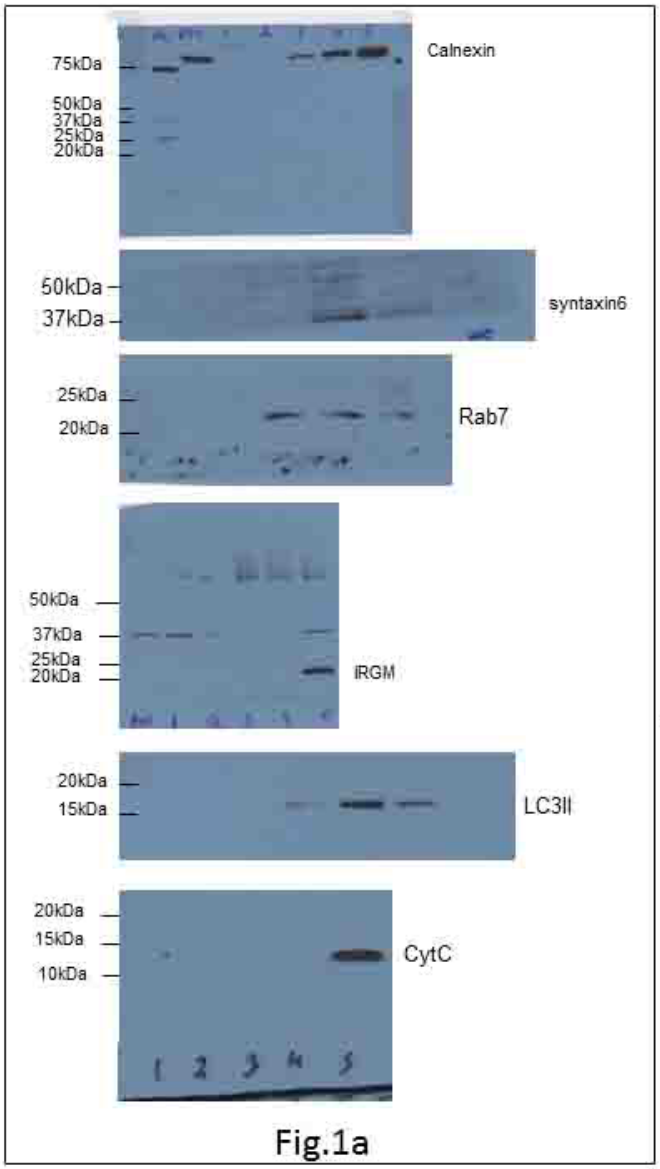

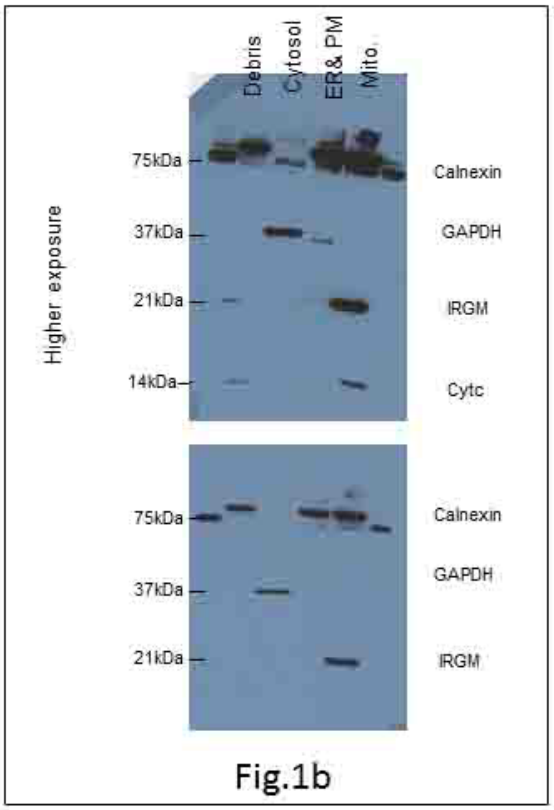

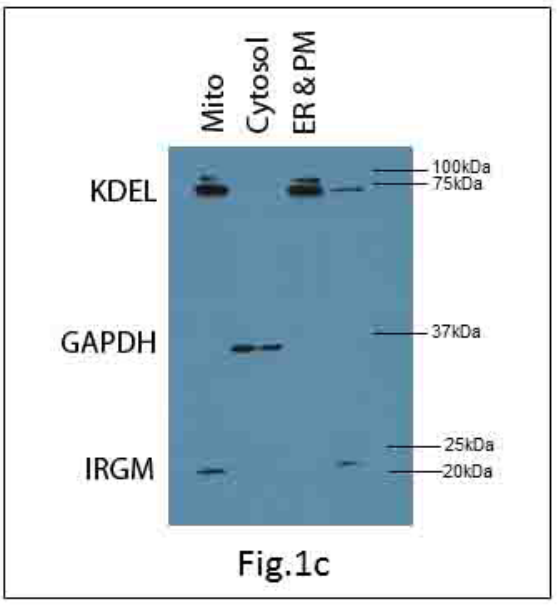

Figure S8 Full length blots corresponding to main text figures as indicated. Self-explanatory.

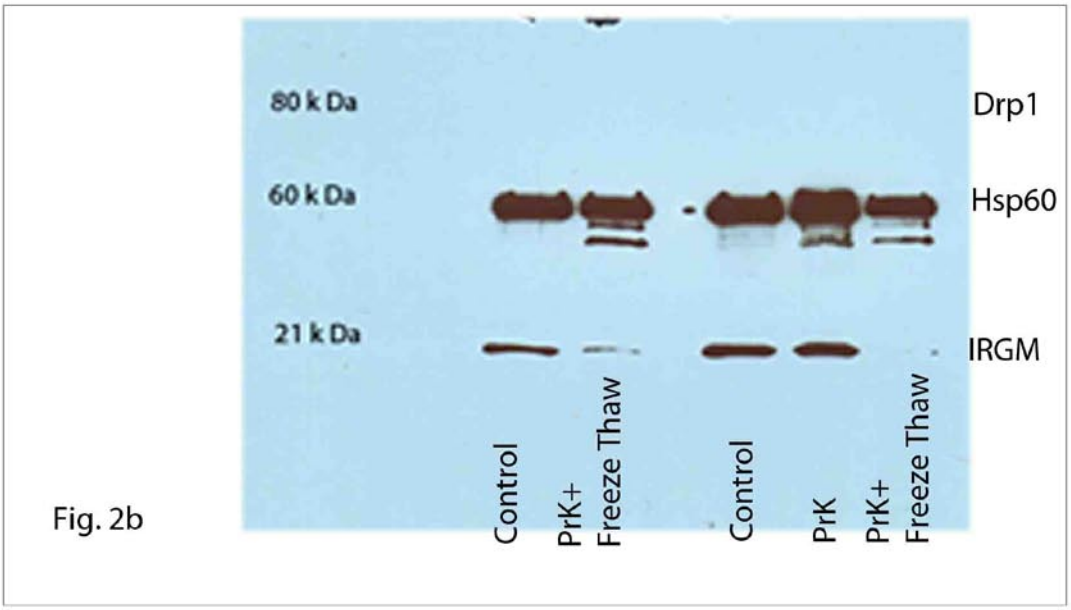

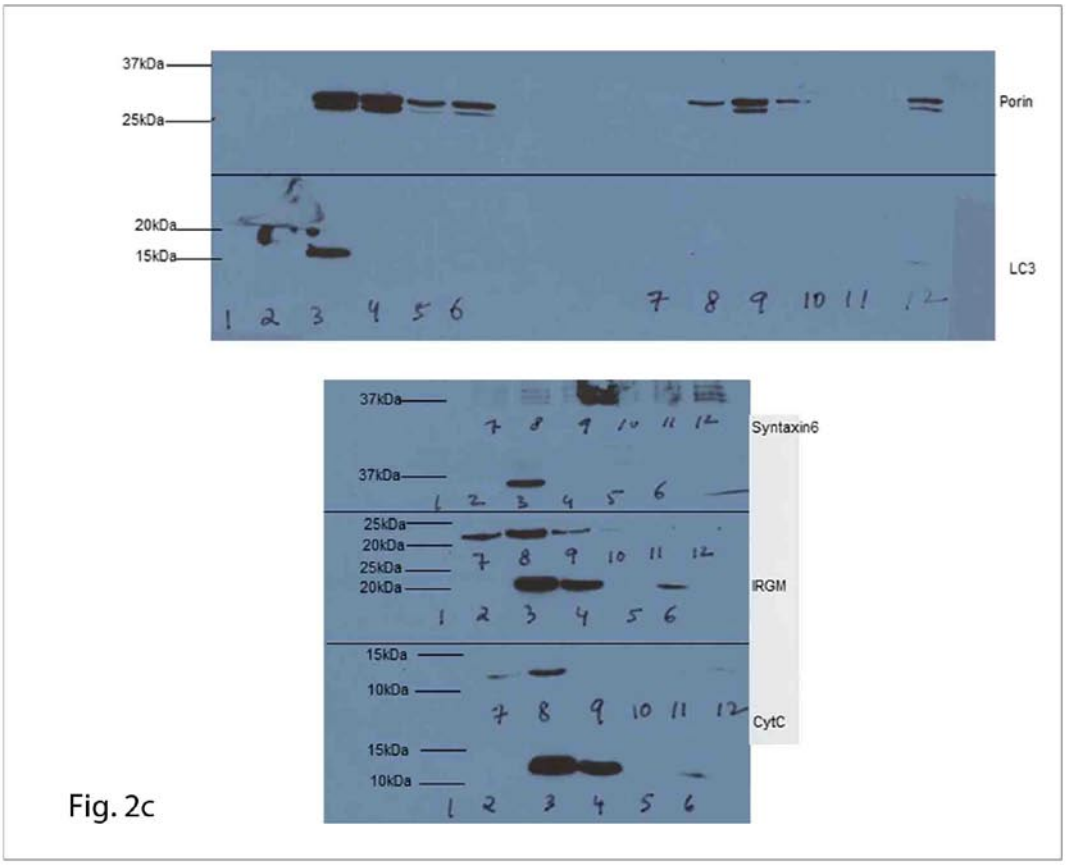

Figure S8 continued

Movie S1 Live microscopy of cells expressing EGFP-IRGMd stained with mitochondrial vital stain MitoTracker Red. 6 hours following transfection, cells were stained with MitoTracker Red and observed by live microscopy using Zeiss 5LIVE microscope, and data analyzed by 4D microscopy as previously described by others [17-20] and us [21-24]. Movie duration: 40 min; frames 1 min apart. Shown is one confocal plane over time.

Supplementary references

1. Detmer, S.A. & Chan, D.C. Functions and dysfunctions of mitochondrial dynamics. Nat Rev Mol Cell Biol 8, 870-879 (2007).
2. Karbowski, M., Jeong, S.Y. & Youle, R.J. Endophilin B1 is required for the maintenance of mitochondrial morphology. The Journal of cell biology 166, 1027-1039 (2004).
3. Niemann, A., Ruegg, M., La Padula, V., Schenone, A. & Suter, U. Ganglioside-induced differentiation associated protein 1 is a regulator of the mitochondrial network: new implications for Charcot-Marie-Tooth disease. The Journal of cell biology 170, 1067-1078 (2005).
4. Ponpuak, M., Delgado, M.A., Elmaoued, R.A. & Deretic, V. Monitoring autophagy during Mycobacterium tuberculosis infection. Methods Enzymol 452, 345-361 (2009).
5. Tasdemir, E. et al. Methods for assessing autophagy and autophagic cell death. Methods in molecular biology (Clifton, N.J 445, 29-76 (2008).
6. Koch, A. et al. Dynamin-like protein 1 is involved in peroxisomal fission. J Biol Chem 278, 8597-8605 (2003).
7. Koch, A., Schneider, G., Luers, G.H. & Schrader, M. Peroxisome elongation and constriction but not fission can occur independently of dynamin-like protein 1. J Cell Sci 117, 3995-4006 (2004).
8. Haines, T.H. A new look at Cardiolipin. Biochimica et biophysica acta 1788, 1997-2002 (2009).
9. Orrenius, S. & Zhivotovsky, B. Cardiolipin oxidation sets cytochrome c free. Nat Chem Biol 1, 188-189 (2005).
10. Schug, Z.T. & Gottlieb, E. Cardiolipin acts as a mitochondrial signalling platform to launch apoptosis. Biochimica et biophysica acta 1788, 2022-2031 (2009).
11. DeVay, R.M. et al. Coassembly of Mgm1 isoforms requires cardiolipin and mediates mitochondrial inner membrane fusion. The Journal of cell biology 186, 793-803 (2009).
12. Tamura, Y., Endo, T., Iijima, M. & Sesaki, H. Ups1p and Ups2p antagonistically regulate cardiolipin metabolism in mitochondria. The Journal of cell biology 185, 1029-1045 (2009).
13. Bekpen, C. et al. Death and resurrection of the human IRGM gene. PLoS Genet 5, e1000403 (2009).
14. Intemann, C.D. et al. Autophagy gene variant IRGM -261T contributes to protection from tuberculosis caused by Mycobacterium tuberculosis but not by M. africanum strains. PLoS Pathog 5, e1000577 (2009).
15. McCarroll, S.A. et al. Deletion polymorphism upstream of IRGM associated with altered IRGM expression and Crohn's disease. Nat Genet 40, 1107-1112 (2008).
16. Singh, S.B., Davis, A.S., Taylor, G.A. & Deretic, V. Human IRGM induces autophagy to eliminate intracellular mycobacteria. Science 313, 1438-1441 (2006).
17. Manders, E.M., Kimura, H. & Cook, P.R. Direct imaging of DNA in living cells reveals the dynamics of chromosome formation. The Journal of cell biology 144, 813-821 (1999).
18. Gerlich, D., Beaudouin, J., Gebhard, M., Ellenberg, J. & Eils, R. Four-dimensional imaging and quantitative reconstruction to analyse complex spatiotemporal processes in live cells. Nature cell biology 3, 852-855 (2001).
19. Platani, M., Goldberg, I., Lamond, A.I. & Swedlow, J.R. Cajal body dynamics and association with chromatin are ATP-dependent. Nature cell biology 4, 502-508 (2002).
20. Gerlich, D. & Ellenberg, J. 4D imaging to assay complex dynamics in live specimens. Nature cell biology Suppl, S14-19 (2003).
21. Chua, J. & Deretic, V. Mycobacterium tuberculosis reprograms waves of phosphatidylinositol 3-phosphate on phagosomal organelles. J Biol Chem 279, 36982-36992 (2004).
22. Vergne, I. et al. Mechanism of phagolysosome biogenesis block by viable Mycobacterium tuberculosis. Proc Natl Acad Sci U S A 102, 4033-4038 (2005).
23. Roberts, E.A., Chua, J., Kyei, G.B. & Deretic, V. Higher order Rab programming in phagolysosome biogenesis. The Journal of cell biology 174, 923-929 (2006).
24. Kyei, G.B. et al. Rab14 is critical for maintenance of Mycobacterium tuberculosis phagosome maturation arrest. The EMBO journal 25, 5250-5259 (2006).